Fluorescent Polymer Nanoparticle for Selective Sensing of Intracellular Hydrogen Peroxide

Wan-Kyu Oh, Yoon Seon Jeong, Sojin Kim, and Jyongsik Jang*

World Class University (WCU) Program of Chemical Convergence for Energy & Environment (C_2E_2), School of Chemical & Biological Engineering, Seoul National University, 599 Gwanangro, Gwanak-gu, Seoul 151-742, Korea

ABSTRACT Fluorescent boronate-modified polyacrylonitrile (BPAN) nanoparticles of 50 nm diameter were fabricated for use as a selective H_2O_2 sensor. The fluorescence intensity changed and an emission peak shifted when BPAN nanoparticles selectively interacted with H_2O_2, relative to other reactive oxygen species (ROS). The BPAN nanoparticles undergo photoinduced electron transfer (PET) between a Schiff base moiety and boronate, which enhances the fluorescence and makes the nanoparticles suitable for selective ROS recognition. We demonstrate the use of these nanoparticles as a detector of endogenous H_2O_2 produced in living cells. The representative features of the fluorescent BPAN nanoparticles that make them particularly attractive for H_2O_2 and ROS detection are the following: they are easily synthesized as PET sensors; they exhibit a characteristic emission peak and peak shift that distinguishes reaction with H_2O_2 from other ROS; and compared to organic compounds, the sensing moiety on BPAN polymer nanoparticles is more thermally stable and has superior mechanical properties, enabling their use in various biomedical applications.

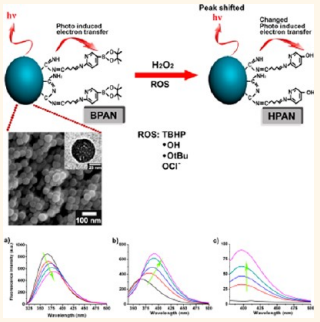

KEYWORDS: fluorescence · hydrogen peroxide detection · nanoparticles · photoinduced electron transfer · polyacrylonitrile · reactive oxygen species

Hydrogen peroxide (H_2O_2), previously known as a byproduct of aerobic respiration and a part of the phagocytic respiratory burst, has recently been shown to be a messenger in cellular signal transduction.[1,2] Overproduction of H_2O_2 and other reactive oxygen species (ROS) can lead to oxidative stress and subsequent functional decline of organ systems, like that observed in neurodegenerative diseases such as Parkinson's and Alzheimer's disease.[3,4] Furthermore, the emerging concept of H_2O_2 as a redox signal that triggers reversible posttranslational modification of precise protein targets has generated interest in understanding how cells produce, partition, and funnel H_2O_2 into specific signaling pathways.[5,6] However, an understanding of the role of H_2O_2 has been elusive due to its low concentration and short lifetime in living cells.[7,8] Therefore, new diagnostic methods are needed to detect and quantify endogenous H_2O_2 production.

Many synthetic fluorescent probes have been recently reported. However, owing to variations in excitation intensity, emission collection efficiency, sample thickness, and/or probe concentration and environment, the application of these probes to quantitative measurements of changes in H_2O_2 concentration in heterogeneous biological samples is complicated.[9,10] Ratiometric fluorescent probes minimize these factors and can provide accurate and quantitative readouts.[11,12] Fluorescent probes using boronate are suitable to study the generation of specific types of ROS in biological systems, as confocal microscopy allows for the use of multiple probes simultaneously in a single specimen, as long as spectral overlap is sufficiently minimized.[13−15]

Here, we report the fabrication of a new fluorescent boronate-modified polyacrylonitrile (BPAN) nanoparticle for use as a selective H_2O_2 sensor. Polyacrylonitrile (PAN) nanoparticles of 50 nm diameter were synthesized using microemulsion polymerization and then further modified to form BPAN nanoparticles. The fluorescence intensity changed and an emission peak shifted when BPAN nanoparticles selectively interacted with H_2O_2, relative to other ROS. The BPAN nanoparticles undergo photoinduced electron transfer (PET) between a Schiff base moiety and boronate, which enhances the fluorescence and makes the nanoparticles suitable for selective molecular recognition. Here, we demonstrate the use of these nanoparticles as a detector of endogenous H_2O_2 produced in living cells. The representative features of the fluorescent BPAN nanoparticles that make them particularly attractive for H_2O_2 and ROS detection are the following: they are easily synthesized as PET sensors; they exhibit a characteristic emission

* Address correspondence to jsjang@plaza.snu.ac.kr.

Received for review December 14, 2011 and accepted September 6, 2012.

Published online September 12, 2012
10.1021/nn204899m

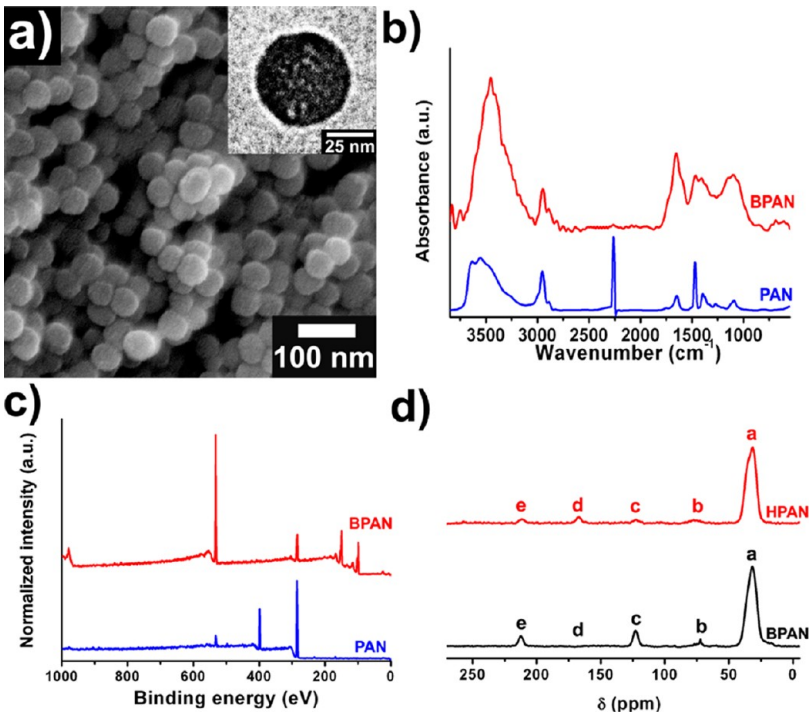

Figure 1. (a) SEM image of BPAN nanoparticles (inset: TEM image of BPAN nanoparticles); (b) FT-IR spectra of PAN (blue line) and BPAN (red line) nanoparticles; (c) XP survey spectra of PAN (blue line) and BPAN (red line) nanoparticles; (d) ^{13}C solid-state NMR spectra of the present BPAN (black line) and HPAN (red line) nanoparticles with CPMAS measurement.

peak and peak shift that distinguishes reaction with H_2O_2 from other ROS; and compared to organic compounds, the sensing moiety on BPAN polymer nanoparticles is more thermally stable and has superior mechanical properties, enabling their use in various biomedical applications.

RESULTS AND DISCUSSION

BPAN nanoparticles were prepared using the procedure displayed in Figure S1. First, 50 nm diameter PAN nanoparticles were fabricated using radical polymerization by dissolving acrylonitrile (AN) monomer in distilled water with a stabilizer. After introducing ammonium persulfate, the radical polymerization of the AN monomer proceeded for 24 h (see Materials and Methods). The PAN nanoparticles were uniform and monodispersed, as determined by scanning electron microscopy (SEM), transmission electron microscopy (TEM), and electrophoretic light scattering (ELS) analysis (Figures 1a and S2). A Schiff base was achieved by surface modification *via* the Pinner method and further aldehyde reaction. Finally, the BPAN nanoparticles were produced upon treatment with 3-aminopyridine-5-boronic acid pinacol ester.

The formation of PAN and BPAN nanoparticles was confirmed by Fourier-transform infrared (FT-IR) spectrometry (Figure 1c and Table S1). The FT-IR spectrum of the PAN nanoparticles shows characteristic PAN peaks, including the C≡N stretching bands at 1446 and 2244 cm^{-1} and the C−H stretching peak at 2872 cm^{-1}.[16,17] These peaks reveal the successful polymerization of PAN by microemulsion polymerization. For the BPAN nanoparticles, peaks related to the boronic acid pinacol ester and Schiff base appeared, including symmetric B−O stretching at 1097 cm^{-1}, asymmetric C−O stretching at 1290 cm^{-1}, B−O stretching at 1402 cm^{-1}, B−C stretching at 1465 cm^{-1}, and the Schiff base peak at 1652 cm^{-1}.[18,19] On the basis of these data, boronic acid pinacol ester successfully modified the nanoparticle surfaces. X-ray photoelectron spectroscopy (XPS) was employed to characterize the surface modification of the PAN nanoparticles (Figures S3−7; see the Supporting Information). XP survey spectra and enlarged C 1s, N 1s, O 1s, and B 1s spectra confirmed the successful fabrication of PAN and BPAN nanoparticles.

To obtain the information on BPAN nanoparticle structure, the present nanoparticles were subjected to ^{13}C solid-state NMR measurement. Figure 1d shows NMR spectra with CPMAS measurement modes. The spectrum of BPAN nanoparticles (black line) represents the expected signals for Schiff base and pyridine boronic acid pinacol ester modification, which can be assigned on the basis of data reported in the previous literature.[20,21] Table S2 summarizes the assignments of the ^{13}C CPMAS spectrum of the BPAN nanoparticles. Briefly, broad signal *a* at 31.9 ppm is assigned to the aliphatic chain of the BPAN. The regions 72.0 and 122.2 ppm (*b* and *c*) are assigned to the Schiff base and pyridine, respectively, and the region 212.6 ppm (*e*) is assigned to boronic acid pinacol ester in the BPAN nanoparticles.

Figure 2 shows selective H_2O_2 sensing *via* fluorescent BPAN nanoparticles. Fluorescent PET sensors

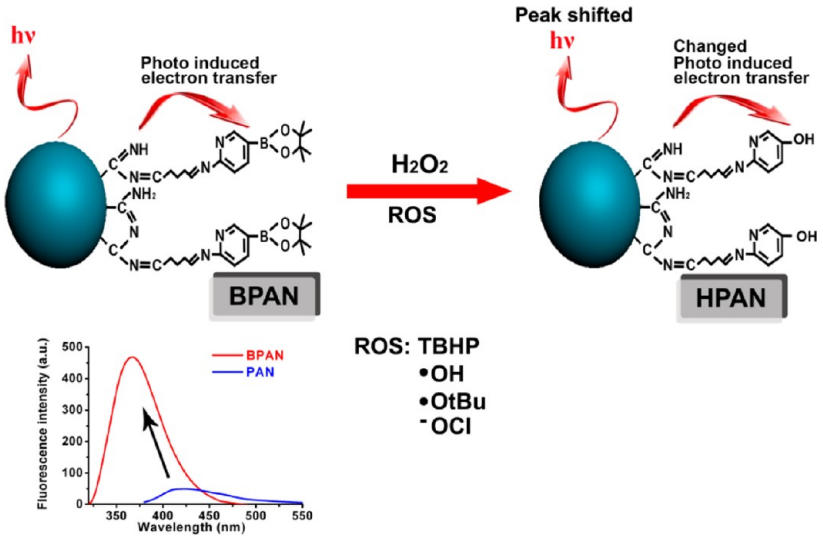

Figure 2. Schematic diagram of H_2O_2 detection using BPAN nanoparticles, and representative fluorescence spectra of PAN (blue line) and BPAN (red line) nanoparticles.

generally include a receptor and a fluorophore separated by a spacer to create a donor–bridge–acceptor system; on the BPAN nanoparticles, this donor–bridge–acceptor system is supplied by the Schiff base group and boronate.[22,23] Figure 2 inset shows representative fluorescence spectra of PAN and BPAN nanoparticles. The fluorescence quantum yield of the PAN nanoparticles (after Schiff base treatment) was calculated as *ca.* 0.10 (blue line; excitation at 360 nm) using the standard reference, 7-amino-4-methylcoumarin.[24] The BPAN nanoparticles showed up to *ca.* 6-fold fluorescence enhancement compared with that of the PAN nanoparticles (red line). Moreover, the excitation/emission (300 nm/376 nm) of the BPAN nanoparticles exhibited blue shifts compared to that of the PAN nanoparticles. This spectral change could be due to efficient electronic communication between the Schiff base and pyridine boronic acid pinacol ester group; for example, the construction of the π-conjugation and PET systems.[25,26]

Reaction with H_2O_2 converts BPAN nanoparticles to H_2O_2-treated (HPAN) nanoparticles, in which some of the boronate groups are replaced by pyridone groups.[27,28] The OH groups of HPAN nanoparticles, in combination with other intraparticle functionalities, such as imine N and deprotonated phenolate O^-, could selectively sequester iron. Owing to this chemospecific deprotection mechanism, boronate derivatives on the BPAN nanoparticles exhibit high selectivity for H_2O_2 over other ROS and can respond to changes in H_2O_2 fluxes at oxidative stress levels. The spectrum of ^{13}C solid-state NMR of the HPAN nanoparticles exhibits the appearance of a characteristic peak at 166.9 ppm (*d*), which is assigned to a pyridone group (Figure 1d; red line).

We evaluated the spectral properties and H_2O_2 response of the new boronated nanoparticles in aqueous buffer at physiological pH (20 mM 4-(2-hydroxyethyl)-1-piperazine-ethanesulfonic acid (HEPES), pH 7; Figure 3). The boronate groups forced the BPAN nanoparticles to adopt a PET form that enhanced fluorescence in the blue region of the spectrum. The addition of H_2O_2 triggered a marked decrease in fluorescence intensity of the BPAN nanoparticles when the excitation wavelength was 300 nm. Moreover, a new emission peak, derived from the Schiff base, dramatically appeared after H_2O_2 treatment when the excitation wavelength was 360 nm. This peak was red-shifted from 365 to 398 nm when the excitation wavelength was 320 nm. These observations provided a simple means to distinguish H_2O_2 from other ROS. The BPAN nanoparticles exhibited ratiometric detection of H_2O_2. The limit of detection values of BPAN nanoparticles for H_2O_2 were 100 pM. This phenomenon is unique among conventional PET sensors and, to the best of our knowledge, has not been previously reported. We presume that intraparticle interactions are responsible for the peak shift and appearance. Additionally, the rate of conversion of BPAN to HPAN nanoparticles was determined by measuring the change in absorption using pseudo-first-order reaction conditions with an excess of H_2O_2. The calculated rate constants indicated that the Schiff base and pyridine linkage in BPAN nanoparticles provided the conversion with a rate constant of 3.59 M^{-1} s^{-1} (Figure S8).

Because of this chemospecific boronate switch and PET effect, the BPAN nanoparticles respond with good selectivity to H_2O_2 over a variety of biologically relevant ROS, including hypochlorite ($^-$OCl), *tert*-butyl hydroperoxide (TBHP), hydroxyl radical (·OH), and *tert*-butoxy radicals (·OtBu) (Figure 4 and Figures S8–16; see Supporting Information). The fluorescence seen at an excitation wavelength of 360 nm was observed only when the BPAN nanoparticles interacted with H_2O_2, not with any other ROS, thus providing highly selective detection. Furthermore, the fluorescence response of the BPAN nanoparticles to H_2O_2 at three separate excitation

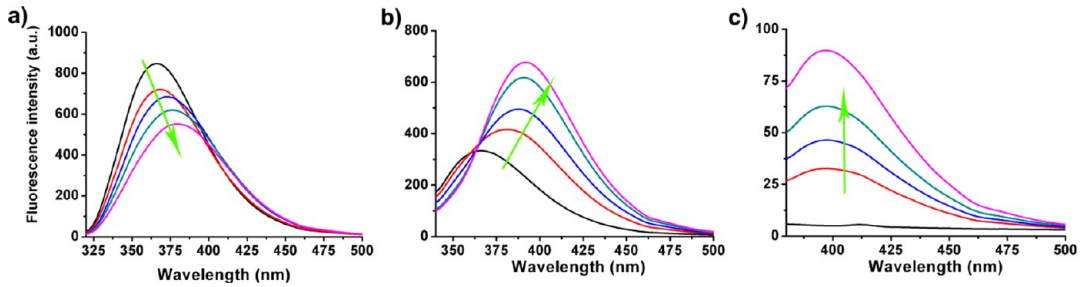

Figure 3. Ratiometric fluorescence spectral changes of 10 μg mL^{-1} BPAN nanoparticles in the presence of H_2O_2 as a function of different excitation wavelength: (a) 300 nm, (b) 320 nm, and (c) 360 nm. Data were acquired at 25 °C in 20 mM HEPES, pH 7, 1 min after the addition of H_2O_2. H_2O_2 concentrations represent 0, 20, 40, 60, and 80 μM.

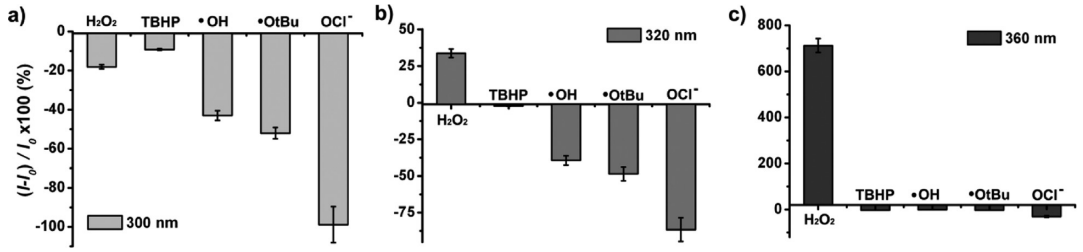

Figure 4. Fluorescence response of 10 μg mL^{-1} BPAN nanoparticle solution in the presence of H_2O_2 and other ROS excited at (a) 300 nm, (b) 320 nm, and (c) 360 nm. Bars exhibit fluorescence changes after addition of each ROS (20 μM) compared with pristine BPAN nanoparticle solution. Data acquired at 25 °C in 20 mM HEPES, pH 7. Emission was collected between (a) 320 and 500 nm; (b) 340 and 500 nm; (c) 380 and 500 nm. Values exhibit mean ± SD, and each experiment was performed in triplicate.

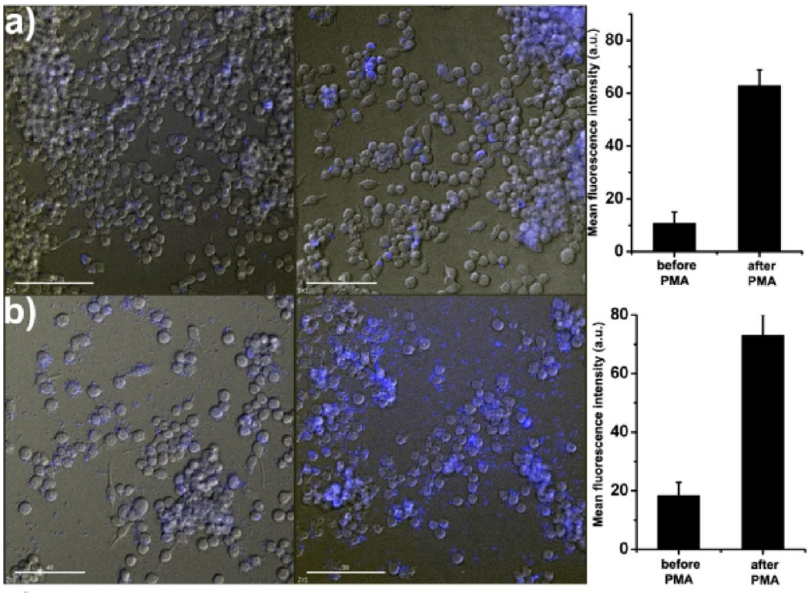

Figure 5. Live cell differential interference images of BPAN-treated RAW264.7 cells: (a) 5 and (b) 10 μg mL^{-1}; left images are before treatment of PMA and right images are 10 min after treatment of 1 μg mL^{-1} PMA. Scale bars = 50 μm. Mean fluorescence intensity values of BPAN-treated RAW264.7 cells: (a) 5 and (b) 10 μg mL^{-1}; left bar represents before treatment of PMA and right bar indicates 10 min after treatment of 1 μg mL^{-1} PMA.

wavelengths was clearly different from the response to other ROS, permitting one to distinguish between H_2O_2 and other biologically relevant ROS. Moreover, the fluorescence change observed at an excitation wavelength of 300 nm upon addition of ROS was ratiometric. These data provide further evidence that H_2O_2-triggered conversion of boronates to phenols is a robust and versatile methodology for reaction-based H_2O_2 detection. The whole sensing procedure took only 1 min, enabling rapid detection of H_2O_2 (Figure S17), which would be considerably advantageous in biomedical applications. The fluorescence intensity of the reaction system barely changed after 1 min, indicating that the reaction product is photostable.

To investigate the *in vitro* application of BPAN nanoparticles, microscopic images were made of

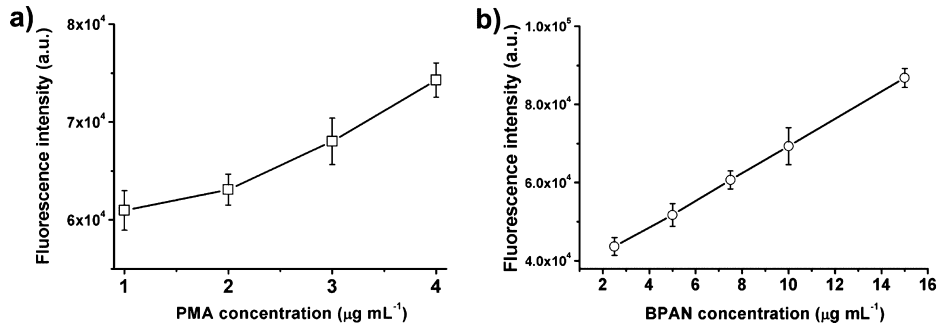

Figure 6. Titration plot of PMA concentration-dependent and BPAN dose-dependent fluorescence alteration in RAW 264.7 cells. (a) Response of 7.5 μg mL^{-1} BPAN nanoparticle-treated cells in the presence of PMA (1, 2, 3, and 4 μg mL^{-1}). (b) Response of BPAN nanoparticle-incubated cells (2.5, 5, 7.5, 10, 15 μg mL^{-1}) after adding 1 μg mL^{-1} PMA.

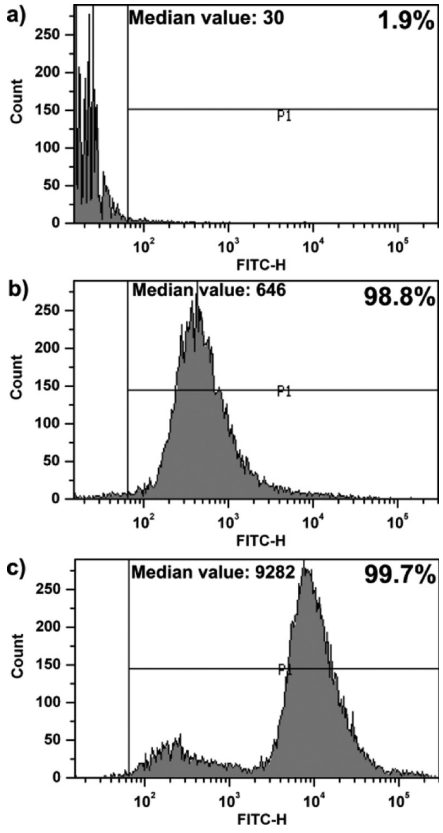

Figure 7. Flow cytometry analyses of particle uptake. Quantification of cellular uptake of (a) negative control, (b) 10 μg mL^{-1}, and (c) 100 μg mL^{-1} FITC-modified PAN nanoparticles. Upper right values are the number of nanoparticle-contained RAW264.7 cells, and upper left median values indicate the amount of nanoparticles taken up.

RAW264.7 cells incubated with 5 and 10 μg mL^{-1} BPAN nanoparticles (Figure 5a and b; left column). Cells with BPAN nanoparticles had no considerable change in cell shape. Blue fluorescence from the BPAN nanoparticles was observed both inside and outside the cells. These macrophages produce superoxide upon stimulation with phorbol-12-myristate-13-acetate (PMA), and superoxide is known to be degraded to H_2O_2 by superoxide dismutase or by spontaneous dismutation.[29] Consequently, BPAN-treated cells were stimulated with 1 μg mL^{-1} PMA for 20 min (Figure 5a and b; right column).

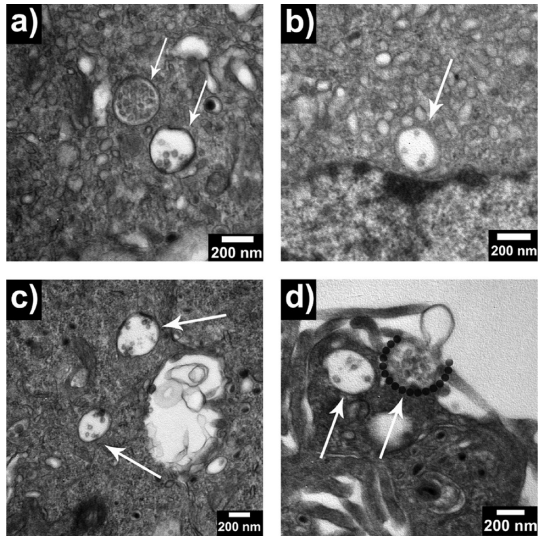

Figure 8. TEM images of RAW264.7 cells incubated with BPAN nanoparticles for 24 h (10 μg mL^{-1}). (a–c) White arrows indicate the nanoparticles that are located in endosomes (scale bar: 200 nm). (d) The nanoparticles are internalized into the cells (gray dotted line indicates invagination of plasma membrane).

The cells treated with PMA exhibited high fluorescence, while macrophages not stimulated with PMA displayed only weak intracellular fluorescence. The mean fluorescence intensity values differed by a factor of *ca.* 4–5 (Figure 5a and b; right graph). The blue-fluorescent BPAN nanoparticles were capable of visualizing endogenous H_2O_2 generation in RAW264.7 cells due to efficient electron transfer after reaction with H_2O_2; the fluorescence from the Schiff base on the HPAN nanoparticles appeared with 360 nm excitation, while the fluorescence from 300 nm excitation decreased. In general, confocal microscopy has a blue filter (ex: 360 nm; em: 457 nm), which is adoptable for this experiment. Judging from these experiments, the BPAN nanoparticles are taken up by the cells and are nontoxic, as well as capable of detecting elevation in H_2O_2 levels under conditions of oxidative stress. The BPAN nanoparticles are sensitive enough to image H_2O_2 produced in RAW264.7 macrophages. This result is consistent with the findings of Abo *et al.* that monoboronate reporters are capable of detecting H_2O_2 in PMA-treated macrophages.[26]

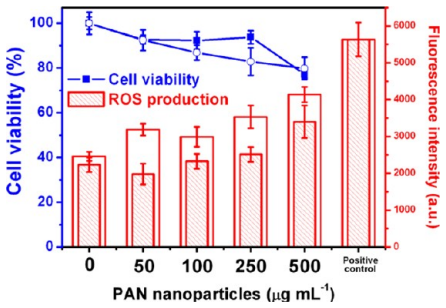

Figure 9. Viability of RAW264.7 cells incubated with PAN (solid squares) and BPAN nanoparticles (open circles) for 24 h. The viability was calculated relative to a negative control. ROS production by RAW264.7 cells after being incubated with PAN (shaded bars) and BPAN nanoparticles (open bars). H_2O_2 (0.02%) was used as a positive control. Values exhibit mean ± SD, and each experiment was performed in triplicate.

Figure 6a shows PMA concentration-dependent fluorescence changes of BPAN nanoparticle-inserted cells (7.5 μg mL^{-1}). As the concentration of inserted PMA increases, inducing hydrogen peroxide from cells grows, resulting in the fluorescence increment. The linear correlation was adjusted as R^2 = 0.93. Figure 6b represents BPAN nanoparticle-dependent fluorescence alteration of the cells in the presence of PMA (1 μg mL^{-1}). The titration plots demonstrate linear correlation between BPAN nanoparticle concentration and fluorescence intensity from the cells (adjusted R^2 = 0.999). As the dose of BPAN nanoparticles increases, generated hydrogen peroxide was more reactive with BPAN nanoparticles. Judging from the data, BPAN nanoparticles are capable of detecting elevation in intracellular hydrogen peroxide, and the detection result is proportional to the quantity of hydrogen peroxide.

Cellular uptake efficiency of the nanoparticles was evaluated by flow cytometry analysis (Figure 7). Fluorescein isothiocyanate (FITC)-modified PAN nanoparticles were used for this experiment due to the restriction of the flow cytometry laser wavelength. RAW264.7 cells were incubated with 10 and 100 μg mL^{-1} nanoparticles for 24 h. Individual intracellular fluorescence intensities were measured *via* flow cytometry, and averages were taken over 10 000 fixed cells to produce an averaged intracellular fluorescence curve. The nanoparticle-internalized cells were calculated as 98.8% and 99.7% for 10 and 100 μg mL^{-1}, respectively. Additionally, fluorescence median values increased from 30 for negative control to 648 and 9282, which indicated the intracellular particles increased with increment with the nanoparticle concentration.

The cellular uptake of the nanoparticles was observed by TEM (Figure 8). In the TEM images, the nanoparticles were clearly located in endosomes (Figure 8a–c). Among various pathways, the nanoparticles were thought to be transported *via* the endosome network, which consists of early endosomes, multivesicular bodies/late endosomes, endolysosomes, and lysosomes.[29] The nanoparticles did not penetrate into nor interact with the mitochondria or the nucleus. Within the cell organelles, the nanoparticles were monodisperse. In Figure 8d, plasma membranes were invaginated to internalize the nanoparticles into cells, which can be denoted as endocytosis.[30]

The viability of RAW264.7 cells with BPAN nanoparticles was determined *in vitro* (Figure 9). To evaluate the number of viable cells, a highly sensitive luminescence assay was conducted based on determination of the adenosine triphosphate (ATP) concentration. The level of ATP production in PAN nanoparticle- and BPAN nanoparticle-treated cells showed no significant decrease compared to a negative control. At a high concentration of nanoparticles (500 μg mL^{-1}), the viability was greater than 80%. To test whether the nanoparticles were generating ROS, we stained PAN- and BPAN-nanoparticle-treated cells for 24 h with 2′,7′-dichlorodihydrofluorescein diacetate (DCF-DA). In the presence of ROS, DCF-DA is promptly oxidized to 2′,7′-dichlorodihydrofluorescein (DCF), resulting in an increase in fluorescence from the cells. As shown in Figure 9, the ROS values are dose-dependent. ROS production was not significantly higher in treated than in untreated cells, and H_2O_2 was less than 0.02%. Therefore, the BPAN nanoparticles are an effective intracellular H_2O_2 detector without significant ROS production. Judging from these data, PAN and BPAN nanoparticles provide ratiometric and selective H_2O_2/ROS detection with low toxicity.

CONCLUSION

We synthesized a novel fluorescent polymeric nanoparticle for use as a probe that can selectively detect H_2O_2 over other competing ROS. A new fluorescence peak appeared when the BPAN nanoparticles reacted with H_2O_2, and this peak shifted with a change in the excitation wavelength. This fluorescence behavior was highly specific for H_2O_2. The use of these novel nanoparticles to detect changes in H_2O_2 concentration was demonstrated in macrophage cells. Considering these observations, the BPAN nanoparticles offer a new way to selectively recognize H_2O_2 and may lead to biomedical applications as an intracellular H_2O_2 sensor.

MATERIALS AND METHODS

Materials. The following chemicals were purchased and used as received: acrylonitrile (Aldrich), decyltrimethylammonium bromide (TCI Korea), ammonium persulfate (Aldrich), hydrogen chloride (Samchun Chemical), diethyl ether (Samchun Chemical), ammonia solution (Aldrich), ethyl alcohol (Samchun Chemical), glutaraldehyde (Aldrich), 1 M phosphate buffer solution (Aldrich), 2-aminopyridine-5-boronic acid pinacol ester (Aldrich), hydrogen peroxide (35 wt % solution in water; Aldrich), *tert*-butyl hydroperoxide solution (70 wt % in solution; Aldrich), sodium hypochlorite solution (Hanawa Chemical pure), iron(III) chloride

(Sigma-Aldrich), iron(II) chloride (Sigma-Aldrich), copper chloride (Aldrich), and zinc chloride (Sigma-Aldrich).

Synthesis of PAN Nanoparticles. The PAN nanoparticles were prepared by a microemulsion templating method. First, decyltrimethylammonium bromide (DeTAB; 2.4 g) was dissolved in distilled water (20 mL). Acrylonitrile (1 g) was added dropwise into the DeTAB solution, and then ammonium persulfate (0.052 g) was inserted into the solution. The microemulsion polymerization proceeded at 70 °C for 24 h. The resulting product was diluted by adding excess ethanol, and subsequently the precipitates were dried in a vacuum oven at room temperature.

Surface Modification of PAN Nanoparticles. To graft boronate on the surface of PAN nanoparticles, Pinner synthesis was employed. A 0.5 g amount of PAN nanoparticles in ethanol (10 mL) was added into 1 M HCl in diethyl ether (20 mL) at 0 °C for 72 h in flasks under N_2 reflux. Then, the product was washed with ethanol and precipitated. The product was treated with ammonia solution (20 mL) under a nitrogen purge for 3 h. The product was washed with ethanol and precipitated for the next step. The product was inserted into 1% glutaraldehyde solution to synthesize the Schiff base. The solution was diluted by distilled water and centrifuged. Subsequently, the product was reacted with 2-aminopyrimidine-5-boronic acid pinacol ester (0.1 M; 2 mL) for 2 h. The resulting BPAN nanoparticles were washed with distilled water and centrifuged (see Figure S1).

Characterization. Transmission electron microscope images were obtained with a JEOL EM-2000 EX II microscope. Scanning electron microscope was performed with a JEOL 6330F at an acceleration voltage of 10 kV. A Bomem MB 100 FT-IR spectrometer was used to characterize the PAN and BPAN nanoparticles. The emission spectra of BPAN nanoparticles were obtained with a JASCO FP-6500 spectrofluorometer. X-ray photoelectron analysis was performed to investigate the chemical composition of the PAN and BPAN nanoparticles using Sigma Probe (ThermoVG, UK) where the photon source was a microfocused monochromator source. The C 1s core level peak was taken as reference at 284.5 eV.

Quantum Yield. The quantum yield of BPAN nanoparticles was determined by a comparison method of the fluorescence emission with the standard reference, 7-amino-4-methylcoumarin (AMC; Aldrich). AMC has been widely used as a blue-emitting dye, which has a high quantum yield (Φ = 0.88) (*J. Comb. Chem.* **2004**, *6*, 604). The fluorescence quantum yield of BPAN nanoparticles was determined by the following formula:

$$\Phi_P = \frac{F_P}{A_P} \times \frac{A_C}{F_C} \times \Phi_C$$

where Φ is the fluorescence quantum yield, F is the integrated fluorescence signal in the emission region, and A is the absorption coefficient at the excitation wavelength. The subscript P indicates BPAN nanoparticles and C indicates AMC.

H_2O_2 and ROS Detection. The fluorescence intensity changes of PAN nanoparticles after Schiff base treatment were monitored at 424 nm (λ_{ex} = 360 nm). In the case of BPAN nanoparticles, the fluorescence was measured at λ_{ex} = 300, 320, 360 nm. A 0.1 M HEPES buffer solution was employed in all experiments. The concentration of the nanoparticles was fixed at 10 μg mL^{-1}. Samples for absorption and emission measurements were contained in 1 cm × 1 cm quartz cuvettes (3.5 mL volume, from Hellma). H_2O_2, TBHP, and OCl^- were diluted from 35, 70, and 5% aqueous solution, respectively. ·OH and ·OtBu were acquired by reaction of 1 mM Fe^{2+} with 100 μM H_2O_2 or 100 μM TBHP, respectively.

Calculation of Rate Constant. The rate of oxidation of BPAN to HPAN was determined under pseudo-first-order conditions with excess H_2O_2. To a 3.0 mL solution of BPAN nanoparticles in 0.1 M PBS buffer at 10 μg mL^{-1} was added H_2O_2 to final concentrations of 20, 40, 60, 80, and 100 μM. Spectra were monitored over 0.5−5 min at room temperature with at least 30 spectra recorded. The change in absorbance at 360 nm was monitored. The negative slope of the linear fit of $\ln[(A - A_{HPAN})/(A_0 - A_{HPAN})]$ *vs* time gives the rate constant k_{obs} (where A_{HPAN} is the absorbance of a 10 μg mL^{-1} sample of the HPAN and A_0 is the initial absorbance of BPAN, respectively). The rate of conversion (k (M^{-1} s^{-1})) was determined from the slope of the line of k_{obs} *vs* [H_2O_2]. The value of k was measured to be 3.59 M^{-1} s^{-1} in accordance with eq 1.

$$\text{Rate} = k[\text{BPAN}][H_2O_2] \quad (1)$$

Cell Culture. RAW 264.7 cells were cultured in Dulbecco's modified Eagle medium with 10% fetal bovine serum, 1% penicillin−streptomycin solution, 4.5 g L^{-1} D-glucose, 300 mg L^{-1} L-glutamine, and 110 mg L^{-1} sodium pyruvate at 37 °C in a 5% CO_2 atmosphere in 75 cm^2 flasks. The cells were subcultured three times per week. All experiments were performed in a clean atmosphere.

Observation of Live RAW264.7 Cells Treated with BPAN Nanoparticles. RAW 264.7 cells were spread at a density of 3000 cells per well, in eight-well Lab-Tek II chambered coverglass (Nunc, Thermo Fisher Scientific, USA) and treated with BPAN nanoparticles (5 and 10 μg mL^{-1}). After 24 h, the medium was removed and the cells were washed twice with 0.1 M PBS. Subsequently, the cells were treated with 1 μM PMA (Sigma) solution for 10 min at 37 °C. The cells were analyzed with a Delta Vision RT imaging system (Applied Precision, Issaquah, WA, USA) under 5% CO_2 at 37 °C. To obtain images, a Cascade II electron multiplying charge-coupled device camera was used.

Titration Assay in Cells. For the titration assay, 8 × 10^3 RAW264.7 cells per well were cultured in black, opaque, 96-well plates and incubated with the BPAN nanoparticles (5, 10, 15, 20, and 30 μg mL^{-1}) for 24 h. Then, PMA (1, 2, 3, and 4 μg mL^{-1}) was added to the cells for 20 min at 37 °C. Fluorescence intensity was detected by Victor^3 multilabel readers (Perkin-Elmer, Boston, MA, USA) at an excitation wavelength of 355 nm and an emission wavelength of 405 nm.

Flow Cytometric Quantification of Cellular Uptake of PAN Nanoparticles. RAW264.7 cells were plated in four-well plates at initial densities of 70 000 in 3 mL of medium and grown for 24 h. PAN nanoparticles were surface-modified with fluorescein isothiocyanate due to restriction of the fluorescence lamp of the flow cytometer. Fresh medium containing nanoparticles (10 and 100 μg mL^{-1} PAN nanoparticles) was added to the cells and incubated for 24 h. All experiments were set up in triplicate. After the PAN nanoparticle incubation, cells were trypsinized and rinsed with 0.1 M PBS. For quantifying cells with the nanoparticles, cells were resuspended in 0.1 M PBS. Nontreated cells served as a negative control; 10 000 cells were analyzed by using FACSAria flow cytometers using 488 nm laser excitation (Becton-Dickinson).

TEM Observation of RAW264.7 Cells Incubated with Nanoparticles. The cellular uptake of the BPAN nanoparticles into RAW264.7 cell lines was observed with TEM. RAW264.7 cells were cultured in sterile culture dishes (Nunc, Thermo Fisher Scientific, USA) for 24 h, and BPAN nanoparticles (25 μg mL^{-1}) were added for another 24 h. Cells were prefixed with 2% paraformaldehyde and 2% glutaraldehyde (modified Karnovsky's fixative) at 4 °C for 4 h. After being washed with 0.05 M cacodylate buffer, cells were postfixed with 1% osmium tetraoxide at 4 °C for 2 h, washed with distilled water, and then stained with 0.5% uranyl acetate at 4 °C overnight. Dehydration was conducted through a graded series of 30, 50, 70, 80, 90, and 100% ethanol and propylene oxide before embedding in Spurr's resin. Then, the cells were treated with 1:1 propylene oxide/Spurr's resin for 2 h. The cells were infiltrated in Spurr's resin at 70 °C for 24 h, and ultramicrotome was conducted. The sections were stained with 2% uranyl aectate and Raynolds' lead citrate. Then, the samples were observed with TEM at 80 kV.

Cell Viability Assay. For cell viability test, a Cell-Titer glow luminescent cell viability assay (Promega, Madison, WI, USA) was carried out as per manufacturer's instruction. This assay is a homogeneous method to estimate the number of viable and metabolically active cells based on quantification of the ATP concentration. The luminescent intensity was detected after adding the same amount of reagent to the medium. This luminescence was formed because of the transformation of beetle luciferin to oxyluciferin by luciferase in the presence of ATP in the cells. The assay was conducted in white, opaque-walled 96-well plates, and the cells were seeded at a density of 3 × 10^3 cells per well. The cells were then incubated with different concentrations of the PAN and BPAN nanoparticles (50, 100, 200, and 250 μg mL^{-1}) for 24 h. After incubation,

supernatant was removed and the cells were washed with 0.1 M PBS solution to remove residual nanoparticles. The luminescent signal was detected by Victor^3 multilabel readers at 595 nm emission.

ROS Evaluation. The generation of superoxide radical and hydrogen peroxide was detected by 2′,7′-dichlorodihydrofluorescein diacetate staining (Invitrogen, Grand Island, NY, USA). Without intracellular ROS, nonoxidized DCF-DA is nonfluorescent. In the prescence of ROS, it is converted to a highly fluorescent DCF derivative. For the ROS assay, 3×10^3 cells per well were cultured in white, opaque, 96-well plates and incubated with the PAN and BPAN nanoparticles (50, 100, 200, and 250 μg mL^{-1}) for 24 h. Then, the samples were washed with 0.1 M PBS solution and treated with 10 μM DCF-DA for 20 min at 37 °C. The cells treated with hydrogen peroxide (0.02% H_2O_2) were used as a positive control. Fluorescent intensity was detected by Victor^3 multilabel readers at an excitation wavelength of 485 nm and an emission wavelength of 535 nm.

Conflict of Interest: The authors declare no competing financial interest.

Acknowledgment. This research was supported by WCU (World Class University) program through the National Research Foundation of Korea funded by the Ministry of Education, Science and Technology (R31-10013).

Supporting Information Available: 1. Schematic diagram of fabrication procedure, 2. ELS analysis, 3. FT-IR analysis, 4. XPS analysis, 5. NMR analysis, 6. calculation of rate constant for oxidation of BPAN nanoparticles, 7. selectivity of ROS using BPAN nanoparticles, and 8. phototoxicity of BPAN nanoparticles. This material is available free of charge *via* the Internet at http://pubs.acs.org.

REFERENCES AND NOTES

1. Jin, H.; Heller, D. A.; Kalbacova, M.; Kim, J.-H.; Zhang, J.; Boghossian, A. A.; Maheshri, N.; Strano, M. S. Detection of Single-Molecule H_2O_2 Signalling from Epidermal Growth Factor Receptor Using Fluorescent Single-Walled Carbon Nanotubes. *Nat. Nanotechnol.* **2010**, *5*, 302–309.
2. Thubagere, A.; Reinhard, B. r. M. Nanoparticle-Induced Apoptosis Propagates through Hydrogen-Peroxide-Mediated Bystander Killing: Insights from a Human Intestinal Epithelium *in Vitro* Model. *ACS Nano* **2010**, *4*, 3611–3622.
3. Leed, M. G. D.; Wolkow, N.; Pham, D. M.; Daniel, C. L.; Dunaief, J. L.; Franz, K. J. Prochelators Triggered by Hydrogen Peroxide Provide Hexadentate Iron Coordination to Impede Oxidative Stress. *J. Inorg. Biochem.* **2011**, *105*, 1161–1172.
4. Dickens, M. G.; Franz, K. J. A Prochelator Activated by Hydrogen Peroxide Prevents Metal-Induced Amyloid β Aggregation. *ChemBioChem* **2010**, *11*, 59–62.
5. Zhan, X.-Q.; Su, B.-Y.; Zheng, H.; Yan, J.-H. Sensing Hydrogen Peroxide Involving Intramolecular Charge Transfer Pathway: A Boronate-Functioned Styryl Dye as a Highly Selective and Sensitive Naked-Eye Sensor. *Anal. Chim. Acta* **2010**, *658*, 175–179.
6. Kim, J.-H.; Patra, C. R.; Arkalgud, J. R.; Boghossian, A. A.; Zhang, J.; Han, J.-H.; Reuel, N. F.; Ahn, J.-H.; Mukhopadhyay, D.; Strano, M. S. Single-Molecule Detection of H_2O_2 Mediating Angiogenic Redox Signaling on Fluorescent Single-Walled Carbon Nanotube Array. *ACS Nano* **2011**, *5*, 7848–7857.
7. Dickinson, B. C.; Huynh, C.; Chang, C. J. A Palette of Fluorescent Probes with Varying Emission Colors for Imaging Hydrogen Peroxide Signaling in Living Cells. *J. Am. Chem. Soc.* **2010**, *132*, 5906–5915.
8. Karton-Lifshin, N.; Segal, E.; Omer, L.; Portnoy, M.; Satchi-Fainaro, R.; Shabat, D. A Unique Paradigm for a Turn-ON Near-Infrared Cyanine-Based Probe: Noninvasive Intravital Optical Imaging of Hydrogen Peroxide. *J. Am. Chem. Soc.* **2011**, *133*, 10960–10965.
9. Wei, Y.; Zhang, Y.; Liu, Z.; Guo, M. A Novel Profluorescent Probe for Detecting Oxidative Stress Induced by Metal and H_2O_2 in Living Cells. *Chem. Commun.* **2010**, *46*, 4472–4474.
10. Setsukinai, K.-i.; Urano, Y.; Kakinuma, K.; Majima, H. J.; Nagano, T. Development of Novel Fluorescence Probes That Can Reliably Detect Reactive Oxygen Species and Distinguish Specific Species. *J. Biol. Chem.* **2003**, *278*, 3170–3175.
11. Benjaminsen, R. V.; Sun, H.; Henriksen, J. R.; Christensen, N. M.; Almdal, K.; Andresen, T. L. Evaluating Nanoparticle Sensor Design for Intracellular pH Measurements. *ACS Nano* **2011**, *5*, 5864–5873.
12. Sapsford, K. E.; Granek, J.; Deschamps, J. R.; Boeneman, K.; Blanco-Canosa, J. B.; Dawson, P. E.; Susumu, K.; Stewart, M. H.; Medintz, I. L. Monitoring Botulinum Neurotoxin A Activity with Peptide-Functionalized Quantum Dot Resonance Energy Transfer Sensors. *ACS Nano* **2011**, *5*, 2687–2699.
13. Miller, E. W.; Tulyathan, O.; Isacoff, E. Y.; Chang, C. J. Molecular Imaging of Hydrogen Peroxide Produced for Cell Signaling. *Nat. Chem. Biol.* **2007**, *3*, 263–267.
14. Van De Bittner, G. C.; Dubikovskaya, E. A.; Bertozzi, C. R.; Chang, C. J. *In Vivo* Imaging of Hydrogen Peroxide Production in a Murine Tumor Model with a Chemoselective Bioluminescent Reporter. *Proc. Natl. Acad. Sci. U. S. A.* **2010**, *107*, 21316–21321.
15. Lee, D.; Khaja, S.; Velasquez-Castano, J. C.; Dasari, M.; Sun, C.; Petros, J.; Taylor, W. R.; Murthy, N. *In Vivo* Imaging of Hydrogen Peroxide with Chemiluminescent Nanoparticles. *Nat. Mater.* **2007**, *6*, 765–769.
16. Oh, W.-K.; Jeong, Y. S.; Song, J.; Jang, J. Fluorescent Europium-Modified Polymer Nanoparticles for Rapid and Sensitive Anthrax Sensors. *Biosens. Bioelectron.* **2011**, *29*, 172–177.
17. Lee, K. J.; Oh, J. H.; Kim, Y.; Jang, J. Fabrication of Photoluminescent-Dye Embedded Poly(Methyl Methacrylate) Nanofibers and Their Fluorescence Resonance Energy Transfer Properties. *Adv. Mater.* **2006**, *18*, 2216–2219.
18. Lee, K. J.; Oh, W. K.; Song, J.; Kim, S.; Lee, J.; Jang, J. Photoluminescent Polymer Nanoparticles for Label-Free Cellular Imaging. *Chem. Commun.* **2010**, *46*, 5229–5231.
19. Harper, J. C.; Polsky, R.; Wheeler, D. R.; Lopez, D. M.; Arango, D. C.; Brozik, S. M. A Multifunctional Thin Film Au Electrode Surface Formed by Consecutive Electrochemical Reduction of Aryl Diazonium Salts. *Langmuir* **2009**, *25*, 3282–3288.
20. Lakshmi, K. J.; Auger, M.; Raap, J.; Lugtenburg, J.; Griffin, R. G.; Herzfeld, J. Internuclear Distance Measurement in a Reaction Intermediate: Solid-State Carbon-13 NMR Rotational Resonance Determination of the Schiff Base Configuration in the M Photointermediate of Bacteriorhodopsin. *J. Am. Chem. Soc.* **1993**, *115*, 8515–8516.
21. Occhiato, E. G.; Galbo, F. L.; Guarna, A. Preparation and Suzuki−Miyaura Coupling Reactions of Tetrahydropyridine-2-boronic Acid Pinacol Esters. *J. Org. Chem.* **2005**, *70*, 7324–7330.
22. Zhang, L.; Kerszulis, J. A.; Clark, R. J.; Ye, T.; Zhu, L. Catechol Boronate Formation and Its Electrochemical Oxidation. *Chem. Commun.* **2009**, *16*, 2151–2153.
23. Lin, J.; Hu, Q. −S.; Xu, M. −H.; Pu, L. A Practical Enantioselective Fluorescent Sensor for Mandelic Acid. *J. Am. Chem. Soc.* **2002**, *124*, 2088–2089.
24. Song, A.; Zhang, J.; Lebrilla, C. B.; Lam, K. S. Solid-Phase Synthesis and Spectral Properties of 2-Alkylthio-6H-pyrano[2,3-f]benzimidazole-6-ones: A Combinatorial Approach for 2-Alkylthioimidazocoumarins. *J. Comb. Chem.* **2004**, *6*, 604–610.
25. Lippert, A. R.; Gschneidtner, T.; Chang, C. J. Lanthanide-Based Luminescent Probes for Selective Time-Gated Detection of Hydrogen Peroxide in Water and in Living Cells. *Chem. Commun.* **2010**, *46*, 7510–7512.
26. Abo, M.; Urano, Y.; Hanaoka, K.; Terai, T.; Komatsu, T.; Nagano, T. Development of a Highly Sensitive Fluorescence Probe for Hydrogen Peroxide. *J. Am. Chem. Soc.* **2011**, *133*, 10629–10637.
27. Charkoudian, L. K.; Pham, D. M.; Franz, K. J. A Pro-Chelator Triggered by Hydrogen Peroxide Inhibits Iron-Promoted Hydroxyl Radical Formation. *J. Am. Chem. Soc.* **2006**, *128*, 12424–12425.

28. Charkoudian, L. K.; Dentchev, T.; Lukinova, N.; Wolkow, N.; Dunaief, J. L.; Franz, K. J. Iron Prochelator BSIH Protects Retinal Pigment Epithelial Cells against Cell Death Induced by Hydrogen Peroxide. *J. Inorg. Biochem.* **2008**, *102*, 2130–2135.
29. Mu, Q.; Broughton, D. L.; Yan, B. Endosomal Leakage and Nuclear Translocation of Multiwalled Carbon Nanotubes: Developing a Model for Cell Uptake. *Nano Lett.* **2009**, *9*, 4370–4375.
30. Corner, S. D.; Schmid, S. L. Regulated Portals of Entry into the Cell. *Nature* **2003**, *422*, 37–44.